LETTER
SPACE PHYSICS

Earth and Planetary Physics
9: 188–193, 2025
doi: 10.26464/epp2024079

Distinct MLT asymmetry of auroral kilometric radiation observed by the FAST satellite

JiaWen Tang[1], Sai Zhang[1,2*], FuLiang Xiao[1,2*], HongMing Yang[3], Si Liu[1,2], YiHua He[1,2], Chang Yang[1,2], YuYue Jin[1,2], ZhouKun Deng[1], Ping Li[1], and Archie James Johnston[3]

[1]School of Physics and Electronic Sciences, Changsha University of Science and Technology, Changsha 410114, China;

[2]Hunan Province Higher Education Key Laboratory of Modeling and Monitoring on the Near-Earth Electromagnetic Environments, Changsha University of Science and Technology, Changsha 410114, China;

[3]School of Electrical and Information Engineering, Changsha University of Science and Technology, Changsha 410114, China

Key Points:

- A systematic study on the distribution of AKR at high latitudes (60°–80°) is presented of the 5-year data from the FAST satellite.
- AKR in the northern (southern) hemisphere occurs more frequently in the regions of MLT = 05–08 and 18–22 (02–05 and 12–17).
- Such MLT asymmetry is related to the direction of the component B_x of the interplanetary magnetic field.

Citation: Tang, J. W., Zhang, S., Xiao, F. L., Yang, H. M., Liu, S., He, Y. H., Yang, C., Jin, Y. Y., Deng, Z. K., Li, P., and Johnston, A. J. (2025). Distinct MLT asymmetry of auroral kilometric radiation observed by the FAST satellite. *Earth Planet. Phys.*, *9*(1), 188–193. http://doi.org/10.26464/epp2024079

Abstract: Auroral Kilometric Radiation (AKR) is a common radio emission, which can contribute to the magnetosphere–ionosphere–atmosphere coupling. Similar emissions have been observed in all magnetic planet magnetospheres of the solar system. In this study, using observations from the FAST satellite from 30 August 1996 to 9 September 2001, the distribution of AKR in altitude = 500–4500 km and invariant latitude (|ILAT|) = 60°–80° has been analyzed. 63045 AKR samples have been identified with ~48% (52%) samples on the dayside (nightside). Of considerable interest, there is a distinct MLT asymmetry with the high occurrence rate in MLT = 05–08 and 18–22 (02–05 and 12–17) in the northern (southern) hemisphere. The distinct MLT asymmetry is associated with the direction of B_x of the interplanetary magnetic field. In addition, the occurrence rate on the nightside clearly increases as the AE^* index increases. This study further enriches the information and understanding of AKR in the magnetosphere as well as other similar radio emissions.

Keywords: asymmetry; auroral kilometric radiation; interplanetary magnetic field

1. Introduction

Auroral Kilometric Radiation (AKR) is a very intense radio emission that has a wavelength of kilometers and is present on Earth, and it is mainly present in the right-hand extraordinary mode (Kurth et al., 1975; Ergun et al., 1998; Zarka, 1998; Zhang S et al., 2024). The interaction between electromagnetic waves and high-energy particles is an important physical process in the magnetosphere (Yang QW et al., 2016; Jin YY et al., 2018; Guo MY et al., 2020; Guan CY et al., 2020; He JB et al., 2021; Yang C et al., 2021; Zhao YW et al., 2022; Li T et al., 2023). Numerous studies have demonstrated that AKR may scatter electrons into the atmosphere or accelerate them to relativistic energy (Summers et al., 2001; Xiao FL et al., 2006; Xiao FL, 2010a; Xiao FL, 2010b; Xiao FL et al., 2011; Zhang S et al., 2020, 2021). Such AKR-driven accelerating (or scattering) can potentially harm spacecrafts (or destroy ozone) (Thorne, 1977; Callis et al., 1998; Baker, 2002; Thorne et al., 2005). Electron Cyclotron Maser Instability (ECMI) is recognized as an essential process in producing AKR and other radio emissions (Wu CS and Lee, 1979; Melrose et al., 1982; Pritchett, 1984; Calvert, 1995; Mutel et al., 2007; Burinskaya, 2013). It has been proved that the source region of AKR is approximately in the invariant latitude (|ILAT|) = 60°–70° and when the magnetic local time (MLT) is from 20 to 24 (Hashimoto, 1984).

Early observations have shown that AKR occurs more frequently in the auroral zone around |ILAT| = 65° and where MLT = 20–24 (Gurnett, 1974; Kurth et al., 1975; Calvert, 1981; Gurnett et al., 1983). Using observations from the GEOTAIL spacecraft, Kasaba et al. (1997) have pointed out that AKR is more active in the winter hemisphere. Observations of Interball-2 satellite have shown that AKR on the dayside is much less than that on the nightside (Hanasz et al., 2003). Xiao FL et al. (2016) have proved that AKR can propagate down to low latitudes from high latitudes using a three-dimensional ray-tracing method. Statistical results from the Arase satellite have presented the asymmetric distributions of AKR in the region of L = 3.0–9.0, magnetic latitude (|MLAT|) =

First author: J. W. Tang, tang.lucy@foxmail.com
Correspondence to: S. Zhang, saizh@126.com
F. L. Xiao, flxiao@126.com
Received 24 SEP 2024; Accepted 13 NOV 2024.
First Published online 02 DEC 2024.

0–40° and MLT = 0–24 (Xiao FL et al., 2022). Statistical results have recently suggested that the annual and seasonal occurrence patterns of AKR are associated with the direction of the interplanetary magnetic field (Li P et al., 2024). Nevertheless, the systematic distributions of AKR around the polar source cavities have not yet been reported so far. Using observations from the FAST satellite from 30 August 1996 to 9 September 2001, the MLT distribution of AKR in the region of altitude (ALT) = 500–4500 km and |ILAT| = 60°–80° is studied.

2. Observations and Statistical Results

2.1 Case Study

The FAST satellite was launched into an ~83° inclination orbit with 350 km perigee and 4175 km apogee in August 1996 (Carlson et al., 1998; Mcfadden et al., 2001). The satellite crossed the auroral zones (which form ovals at ~65°–70° magnetic latitude North and South) four times during an orbit. The electric field Power Spectral Density (PSD) of AKR is measured by the Plasma Wave Tracker onboard the FAST satellite, which explores the electric field component of the plasma wave in a frequency range from DC to ~2 MHz (Carlson et al., 1998; Ergun et al., 2001). In this study, the acf field data from NASA website is considered.

Figure 1 shows four AKR events observed by the FAST satellite on the dayside and nightside of both hemispheres. In event A (Figures 1a and 1b), the AKR primarily occurs in the 3–7 MLT region of the northern hemisphere, when the sunward component (B_x) of the interplanetary magnetic field (IMF) remains almost positive. In event B (Figures 1c and 1d), the AKR mainly stays in the 19–23 MLT region of the northern hemisphere, when B_x remains almost negative. In event C (Figures 1e and 1f), the AKR primarily stays in the 4–5 MLT region of the southern hemisphere, when B_x remains almost positive. In event D (Figures 1g and 1h), the AKR primarily occurs in the 14–19 MLT region of the southern hemisphere, when B_x remains almost negative. These observations suggest that the distribution of AKR may exhibit MLT asymmetry and the asymmetry is probably associated with the direction of B_x. The asymmetry in two hemispheres and its relation to IMF will be analyzed carefully in the following.

2.2 Statistical Analysis

It has been demonstrated by simulations and observations that AKR emissions typically take place in the right-hand extraordinary (R-X) mode. The local cutoff frequency of R-X mode can be obtained by the local electron gyrofrequency (f_{ce}) and the electron plasma frequency (f_{pe}): $f_{cut} = [f_{ce} + (f_{ce}^2 + 4f_{pe}^2)^{1/2}]/2$. Distinct emissions (PSD ≥ 10^{-14} mV^2 m^{-2} Hz^{-1}) with the frequency above 30 kHz and f_{cut} are identified as AKR emissions. Bins are set with the resolution 500 km in ALT, 1 hour in MLT and 1° in ILAT. In total, there are 38400 bins in the region of ALT = 500–4500 km, |ILAT| = 60°–80° and MLT = 0–24. Using the previous method (Xiao FL et al., 2022), 63045 AKR samples during the period with 30161 (32884) samples on the dayside (nightside). The most (49) samples occur in the bin of ALT = 4000–4100 km, ILAT = 61°–62° and

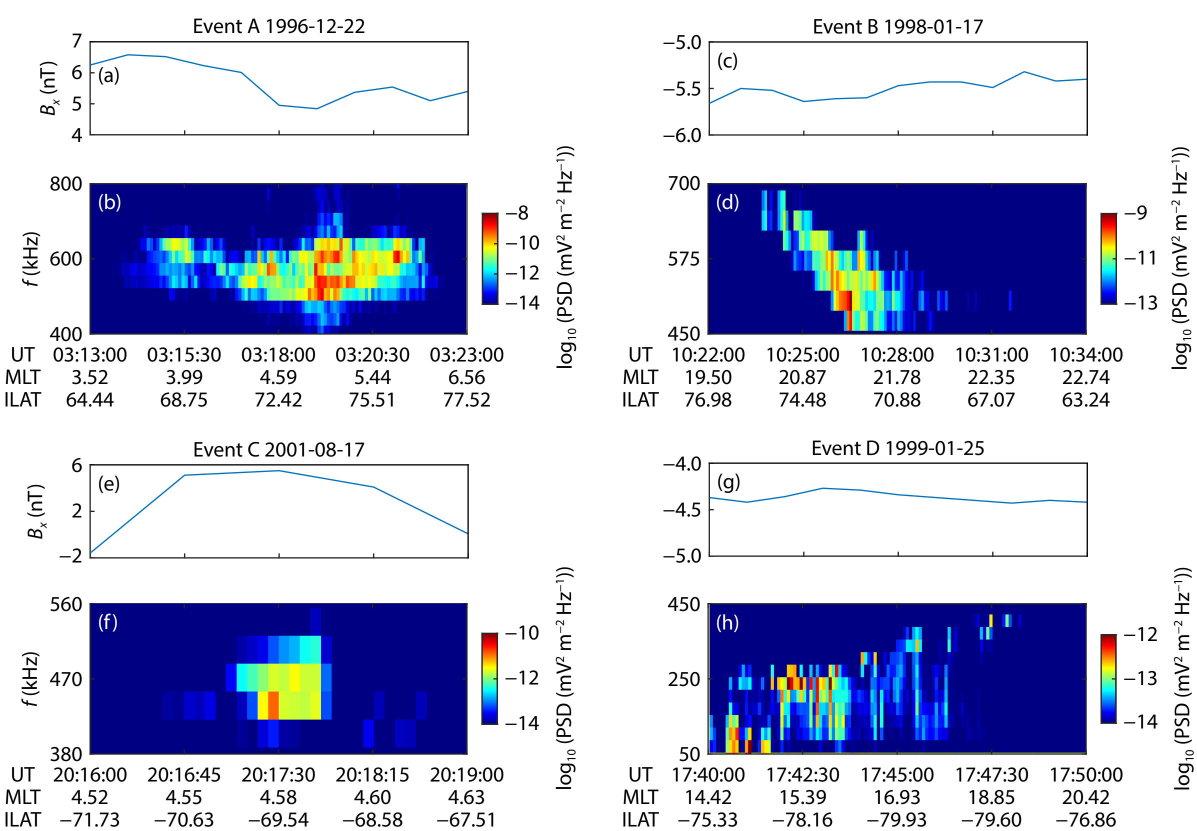

Figure 1. Four AKR events observed by the FAST satellite. (a) Event A observed on UT 03:13:00–03:23:00 1996-12-22. (b) Event B observed on UT 10:22:00–10:34:00 1998-01-17. (c) Event C observed on UT 20:16:00–20:19:00 2001-08-17. (d) Event D observed on UT 17:40:00–17:50:00 1999-01-25.

MLT = 20–21. There are no (or zero) samples in 3783 bins where AKR emissions were not observed. For one orbit, a count of one satellite passing in each bin is recorded. The total number of satellite passing is then counted in each bin for all orbits during the period. For one specific region, the calculated total number of samples (S1) and the total number of satellite passages (S2) in all bins of this region are produced. The occurrence rate of this region is the ratio of S1 to S2. There are 38920 (24125) samples in all bins of the northern (southern) hemisphere, and 288688 (187540) satellite passing in all bins of the northern (southern) hemisphere. The occurrence rate in the northern (southern) hemisphere is 13.48% (12.86%).

In Figure 2a, the number of AKR samples is plotted for each region with the interval of 500 km in ALT and 1 hour in MLT for the whole |ILAT| (60°–80°). There are the most samples in the region of ALT = 3500–4000 km, because the FAST satellite is more frequently in this altitude region. In Figure 2b, the plot of the corresponding occurrence rate is presented. The occurrence rate increases with the increasing altitude and can reach 30% at ALT = 4000–4500 km, because the FAST satellite passes fewer times through this altitude region.

Figure 3a (3b) shows the number (occurrence rate) of AKR samples in the northern hemisphere as a function of MLT and ILAT. The most (590) samples can be observed in the region of

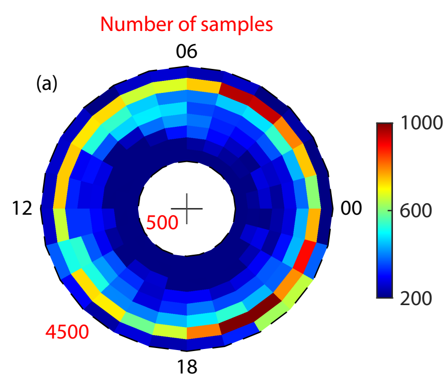

Figure 2. Statistical results of AKR samples observed by the FAST satellite from 30 August 1996 to 9 September 2001. (a) The number of AKR samples for each region with the interval of 500 km in ALT and 1 hour in MLT for the whole |ILAT| = (60°–80°). (b) The occurrence rate of AKR for each region with the interval of 500 km in ALT and 1 hour in MLT for the whole |ILAT| = (60°–80°).

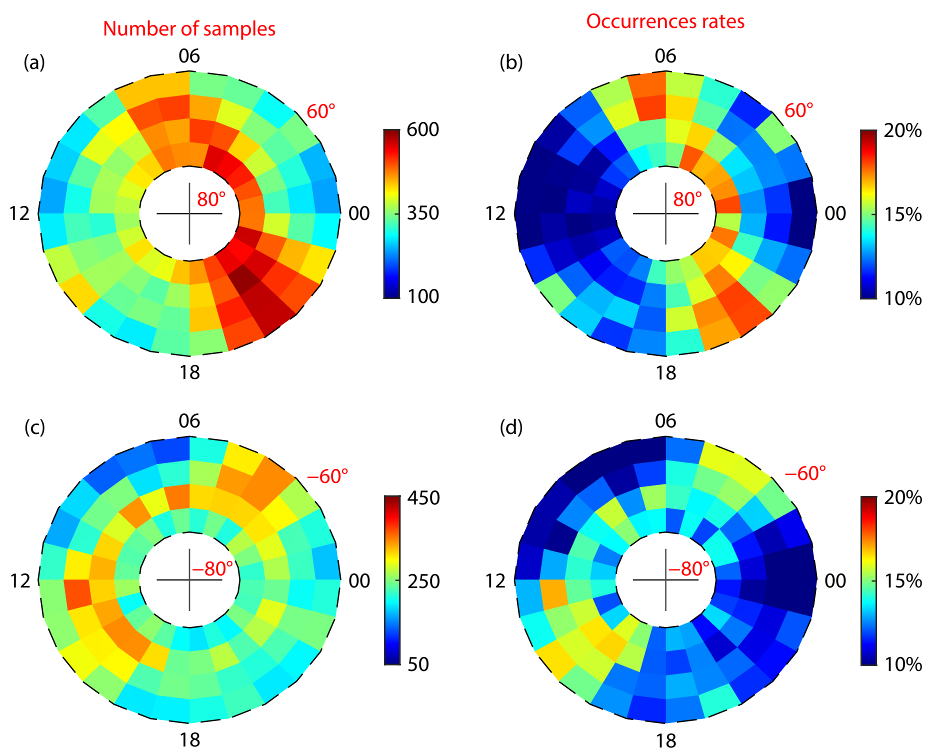

Figure 3. Statistical results of AKR samples as a function of MLT and ILAT in two hemispheres. (a) The number of AKR samples for each region with the interval of 5° in ILAT and 1 hour in MLT in the northern hemisphere. (b) The occurrence rate of AKR samples in the northern hemisphere. (c–d) The same as (a–b) except for the southern hemisphere.

MLT = 20–21 and ILAT = 70°–75°. The relatively high occurrence rates (>15%) primarily stay in the regions of MLT = 04–08 and 19–23. Figure 3c (3d) shows the number (occurrence rate) of AKR samples in the southern hemisphere. The most (368) samples can be observed in the region of MLT = 12–13 and |ILAT| = 65°–70°. The relatively high occurrence rates (>15%) primarily stay in MLT = 02–05 and 12–17. The highest occurrence rate is 18.1% in the region of MLT = 06–07 and ILAT = 65°–70° in the northern hemisphere, or 17% in MLT = 12–13 and |ILAT| = 65°–70° in the southern hemisphere. Furthermore, the regions with relatively high occurrence rates (>16%) in the northern hemisphere are broader than those in the southern hemisphere. The above results show that the MLT distributions of AKR in both hemispheres are clearly asymmetric.

Recent work has demonstrated that the distributions of AKR in two hemispheres are associated with the direction of IMF (Li P et al., 2024). In order to study the correlation between the MLT asymmetry and the direction of B_x, we selected these regions with high occurrence rate for comparative analysis. In Figure 4, the number of samples under different directions of the sunward component (B_x) of IMF in four regions with the high occurrence rate is plotted. In the region of MLT = 05–08 (02–05) of the northern (southern) hemisphere, there are 2572 (1711) samples observed for $B_x > 0$ and 2545 (1679) samples for $B_x < 0$. In the region of MLT = 18–22 (12–17) of the northern (southern) hemisphere, there are 3881 (2733) samples observed for $B_x < 0$ and 3683 (2491) samples for $B_x > 0$. The basic reason for this is that the magnetic reconnection occurs on the dayside magnetopause in one hemisphere and behind the cusp in another hemisphere under the different directions of B_x. More specifically, for $B_x > 0$ (or $B_x < 0$), the magnetic reconnection tends to occur in the dawn of the northern hemisphere and after-midnight of the southern hemisphere (or pre-midnight of the northern hemisphere and afternoon of the southern hemisphere) (Pi G et al., 2018; Lu JY et al., 2021; Wang ZW et al., 2022). Under the drive of the magnetic reconnection, more suprathermal electrons are injected into the polar cavities of the corresponding MLT regions, generating more AKRs.

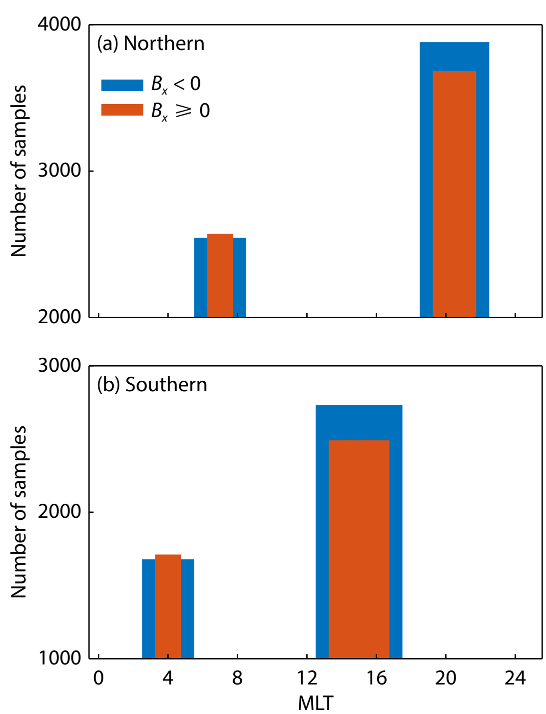

Figure 4. Number of samples under different directions of B_x in four regions with high occurrence rate. (a) Statistical results in the regions of MLT = 05–08 and 18–22 in the northern hemisphere. (b) Statistical results in the regions of MLT = 02–05 and 12–17 in the southern hemisphere.

Figure 5 plots the occurrence rates in both hemispheres as a function of ILAT and MLT under different AE^* indexes. It takes time for the process from the onset of substorms to particle injection, and subsequently to the excitation of emissions. So we adopt AE^* index to characterize the level of geomagnetic activity, which is more precise. The corresponding AE^* index is the mean value of AE index over the previous 1 hour and is recorded for each sample. In both hemispheres, the occurrence rate of AKR increases as the AE^* index increases, typically on the nightside. This is because more suprathermal electrons move into polar source cavities during the strong geomagnetic activity, providing more free energy for the generation of AKR. However, due to the distribution of AE observatories, there is a more notable increase in occurrence rate in the northern hemisphere, compared to the southern hemisphere.

3. Summary

In this study, the MLT distribution characteristics of AKR near source regions using observations from the FAST satellite are presented. 63045 samples are analyzed in the region of ALT = 500–4500 km, |ILAT| = 60°–80° and MLT = 0–24 from 30 August 1996 to 9 September 2001. It might be noted that the occurrence rate is the ratio of the number of AKR samples and the number of satellite passing. The main conclusions are summarized as below:

(1) The relatively high occurrence rates (>15%) for AKR in the northern hemisphere (southern hemisphere) primarily stay in the regions of MLT = 05–08 and 18–22 (02–05 and 12–17), displaying a distinct MLT asymmetry.

(2) The distinct MLT asymmetry of AKR is related to the direction of the component B_x of IMF. Under the condition of $B_x > 0$ (or $B_x < 0$), the magnetic reconnection favorably occurs in the dusk of the southern hemisphere and after-midnight of the northern hemisphere (or pre-midnight of the southern hemisphere and afternoon of the northern hemisphere). Consequently, more suprathermal electrons are injected into the polar cavities of the corresponding MLT regions, producing more AKRs.

(3) In both hemispheres, the occurrence rate of AKR clearly increases with the increasing geomagnetic activity. This is because there are more suprathermal electrons injected into polar source cavities thereby providing more free energy for the generation of AKR.

4. Open Research

Science data of the FAST satellite was obtained from NASA Goddard Space Flight Center for NASA, USA (https://spdf.gsfc.nasa.gov/pub/data/fast/, Carlson et al., 1998). The present study analyzed AC Field-acf-k0 v01 data (doi: 10.48322/23b9-6g23). The

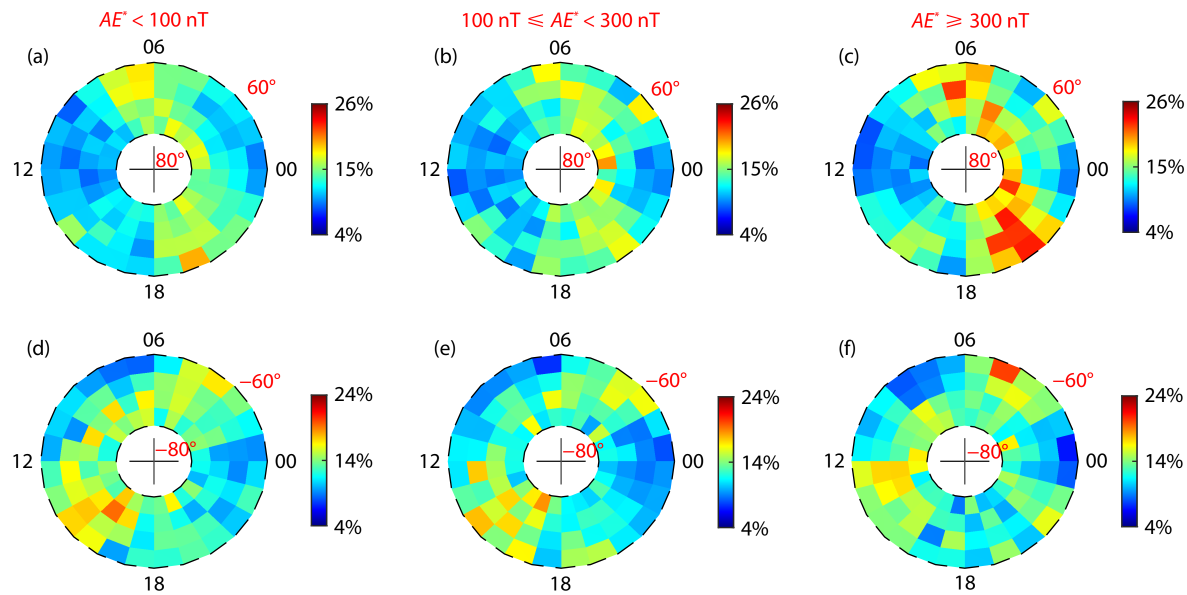

Figure 5. The occurrence rate as a function of MLT and ILAT under different AE^* indexes in two hemispheres. (a–c) The occurrence rate of AKR in the northern hemisphere for AE^* < 100 nT, 100 nT ≥ AE^* < 300 nT and AE^* ≥ 300 nT. (d–f) The same as (a–c) except for the southern hemisphere.

IMF data was downloaded from https://spdf.gsfc.nasa.gov/pub/data/omni/. The *AE* index data was downloaded from http://wdc.kugi.kyoto-u.ac.jp/aeasy/index.html.

Acknowledgments
This work is supported by the National Natural Science Foundation of China grants 42230209, 42374215, 42304183, 72342001, 71931003 and 72061147004; the Scientific Research Fund of Hunan Provincial Education Department grants 21A0212; the Science and Technology Innovation Program of Hunan Province under Grants 2022RC4025, 2023JJ50312, 2023JJ50010.

References

Baker, D. N. (2002). How to cope with space weather. *Science*, *297*(5586), 1486–1487. https://doi.org/10.1126/science.1074956

Burinskaya, T. M. (2013). Ray tracing model of the auroral kilometric radiation generation in the 3-D plasma cavity. *Ann. Geophys.*, *31*(10), 1645–1652. https://doi.org/10.5194/angeo-31-1645-2013

Callis, L. B., Natarajan, M., Evans, D. S., and Lambeth, J. D. (1998). Solar atmospheric coupling by electrons (SOLACE): 1. Effects of the May 12, 1997 solar event on the middle atmosphere. *J. Geophys. Res.: Atmos.*, *103*(D21), 28405–28419. https://doi.org/10.1029/98JD02408

Calvert, W. (1981). The auroral plasma cavity. *Geophys. Res. Lett.*, *8*(8), 919–921. https://doi.org/10.1029/GL008i008p00919

Calvert, W. (1995). An explanation for auroral structure and the triggering of auroral kilometric radiation. *J. Geophys. Res. : Space Phys.*, *100*(A8), 14887–14894. https://doi.org/10.1029/95JA00523

Carlson, C. W., Pfaff, R. F., and Watzin, J. G. (1998). The fast auroral SnapshoT (FAST) mission. *Geophys. Res. Lett.*, *25*(12), 2013–2016. https://doi.org/10.1029/98GL01592

Ergun, R. E., Carlson, C. W., McFadden, J. P., Mozer, F. S., Delory, G. T., Peria, W., Chaston, C. C., Temerin, M., Elphic, R., ... Kistler, L. (1998). FAST satellite wave observations in the AKR source region. *Geophys. Res. Lett.*, *25*(12), 2061–2064. https://doi.org/10.1029/98GL00570

Ergun, R. E., Carlson, C. W., Mozer, F. S., Delory, G. T., Temerin, M., McFadden, J. P., Pankow, D., Abiad, R., Harvey, P., ... Cattell, C. A. (2001). The FAST satellite fields instrument. *Space Sci. Rev.*, *98*(1), 67–91. https://doi.org/10.1023/A:1013131708323

Guan, C. Y., Shang, X. J., Xie, Y. Q., Yang, C., Zhang, S., Liu, S., and Xiao, F. L. (2020). Generation of simultaneous H^+ and He^+ band EMIC waves in the nightside radiation belt. *Sci. China Technol. Sci.*, *63*(11), 2369–2374. https://doi.org/10.1007/s11431-019-1545-6

Guo, M. Y., Zhou, Q. H., Xiao, F. L., Liu, S., He, Y. H., and Yang, C. (2020). Upward propagation of lightning-generated whistler waves into the radiation belts. *Sci. China Technol. Sci.*, *63*(2), 243–248. https://doi.org/10.1007/s11431-018-9486-9

Gurnett, D. A. (1974). The Earth as a radio source: Terrestrial kilometric radiation. *J. Geophys. Res.*, *79*(28), 4227–4238. https://doi.org/10.1029/JA079i028p04227

Gurnett, D. A., Shawhan, S. D., and Shaw, R. R. (1983). Auroral hiss, *Z* mode radiation, and auroral kilometric radiation in the polar magnetosphere: DE 1 observations. *J. Geophys. Res.: Space Phys.*, *88*(A1), 329–340. https://doi.org/10.1029/ja088ia01p00329

Hanasz, J., Panchenko, M., de Feraudy, H., Schreiber, R., and Mogilevsky, M. M. (2003). Occurrence distributions of the auroral kilometric radiation ordinary and extraordinary wave modes. *J. Geophys. Res.: Space Phys.*, *108*(A11), 1408. https://doi.org/10.1029/2002JA009579

Hashimoto, K. (1984). A reconciliation of propagation modes of auroral kilometric radiation. *J. Geophys. Res.: Space Phys.*, *89*(A9), 7459–7466. https://doi.org/10.1029/JA089iA09p07459

He, J. B., Jin, Y. Y., Xiao, F. L., He, Z. G., Yang, C., Xie, Y. Q., He, Q., Wang, C. Z., Shang, X. J., ... Zhang, S. (2021). The influence of various frequency chorus waves on electron dynamics in radiation belts. *Sci. China Technol. Sci.*, *64*(4), 890–897. https://doi.org/10.1007/s11431-020-1750-6

Jin, Y. Y., Yang, C., He, Y. H., Liu, S., Zhou, Q. H., and Xiao, F. L. (2018). Butterfly distribution of Earth's radiation belt relativistic electrons induced by dayside chorus. *Sci. China Technol. Sci.*, *61*(2), 212–218. https://doi.org/10.1007/s11431-017-9067-y

Kasaba, Y., Matsumoto, H., Hashimoto, K., and Anderson, R. R. (1997). The angular distribution of auroral kilometric radiation observed by the geotail spacecraft. *Geophys. Res. Lett.*, *24*(20), 2483–2486. https://doi.org/10.1029/97GL02599

Kurth, W. S., Baumback, M. M., and Gurnett, D. A. (1975). Direction-finding measurements of auroral kilometric radiation. *J. Geophys. Res.*, *80*(19), 2764–2770. https://doi.org/10.1029/JA080i019p02764

Li, P., Zhang, S., Xiao, F. L., Yang, H. M., Ye, S. Y., Liu, S., He, Y. H., Yang, Q. W., Tang, J. W., and Johnston, A. J. (2024). Annual and seasonal occurrence pattern of auroral kilometric radiation associated with the interplanetary magnetic field. *Astrophys. J. Lett.*, *966*(2), L26. https://doi.org/10.3847/2041-8213/ad40a7

Li, T., Liu, S., Yang, C., Xiao, F. L., Yang, H. M., Zhang, S., Gao, Z. L., He, Q., Zhou, Q. H., ... He, Y. H. (2023). Direct evidence for efficient scattering of suprathermal electrons by whistler mode waves in the Martian magnetosphere. *Earth Planet. Phys.*, *7*(6), 607–614. https://doi.org/10.26464/epp2023086

Lu, J. Y., Zhang, H. X., Wang, M., Kabin, K., Zhou, Y., and Li, J. Y. (2021). Energy transfer across the magnetopause under radial IMF conditions. *Astrophys. J.*, *920*(1), 52. https://doi.org/10.3847/1538-4357/ac15f4

McFadden, J. P., Ergun, R. E., Carlson, C. W., Herrick, W., Loran, J., Vernetti, J., Teitler, W., Bromund, K., and Quinn, T. (2001). Science operations and data handling for the fast satellite. *Space Sci. Rev.*, *98*(1), 169–196. https://doi.org/10.1023/A:1013179624253

Melrose, D. B., Rönnmark, K. G., and Hewitt, R. G. (1982). Terrestrial kilometric radiation: The cyclotron theory. *J. Geophys. Res. : Space Phys.*, *87*(A7), 5140–5150. https://doi.org/10.1029/ja087ia07p05140

Mutel, R. L., Peterson, W. M., Jaeger, T. R., and Scudder, J. D. (2007). Dependence of cyclotron maser instability growth rates on electron velocity distributions and perturbation by solitary waves. *J. Geophys. Res.: Space Phys.*, *112*(A7), A07211. https://doi.org/10.1029/2007ja012442

Pi, G., Němeček, Z., Šafránková, J., Grygorov, K., and Shue, J. H. (2018). Formation of the dayside magnetopause and its boundary layers under the radial IMF. *J. Geophys. Res. : Space Phys.*, *123*(5), 3533–3547. https://doi.org/10.1029/2018JA025199

Pritchett, P. L. (1984). Relativistic dispersion, the cyclotron maser instability, and auroral kilometric radiation. *J. Geophys. Res.: Space Phys.*, *89*(A10), 8957–8970. https://doi.org/10.1029/JA089iA10p08957

Summers, D., Thorne, R. M., and Xiao, F. L. (2001). Gyroresonant acceleration of electrons in the magnetosphere by superluminous electromagnetic waves. *J. Geophys. Res.: Space Phys.*, *106*(A6), 10853–10868. https://doi.org/10.1029/2000JA000309

Thorne, R. M. (1977). Energetic radiation belt electron precipitation: A natural depletion mechanism for stratospheric ozone. *Science*, *195*(4275), 287–289. https://doi.org/10.1126/science.195.4275.287

Thorne, R. M., O'Brien, T. P., Shprits, Y. Y., Summers, D., and Horne, R. B. (2005). Timescale for MeV electron microburst loss during geomagnetic storms. *J. Geophys. Res.: Space Phys.*, *110*(A9), A09202. https://doi.org/10.1029/2004JA010882

Wang, Z. W., Lu, J. Y., Hu, H. Q., Liu, J. J., Hu, Z. J., Wang, M., Li, B., Chen, X. C., Wu, Y. W., ... Guan, H. Y. (2022). HMB variations measured by SuperDARN during the extremely radial IMFs: Is the coupling function applicable in radial IMF?. *J. Geophys. Res. : Space Phys.*, *127*(2), e2021JA029589. https://doi.org/10.1029/2021JA029589

Wu, C. S., and Lee, L. C. (1979). A theory of the terrestrial kilometric radiation. *Astrophys. J.*, *230*, 621–626. https://doi.org/10.1086/157120

Xiao, F. L., He, H. Y., Zhou, Q. H., Zheng, H. N., and Wang, S. (2006). Relativistic diffusion coefficients for superluminous (auroral kilometric radiation) wave modes in space plasmas. *J. Geophys. Res.: Space Phys.*, *111*(A11), A11201. https://doi.org/10.1029/2006JA011865

Xiao, F. L., Chen, L. X., He, Y. H., and Yang, C. (2010a). Dynamic evolution of outer radiation belt electrons driven by superluminous R-X mode waves. *Sci. China Technol. Sci*, *53*(10), 2734–2738. https://doi.org/10.1007/s11431-010-4071-8

Xiao, F. L., Su, Z. P., Chen, L. X., Zheng, H. N., and Wang, S. (2010b). A parametric study on outer radiation belt electron evolution by superluminous R-X mode waves. *J. Geophys. Res.: Space Phys*, *115*(A10), A10217. https://doi.org/10.1029/2010JA015374

Xiao, F. L., Chen, L. X., and He, Y. H. (2011). Bounce-averaged diffusion coefficients for superluminous wave modes in the magnetosphere. *J. Atmos. Sol.-Terr. Phys.*, *73*(1), 88–94. https://doi.org/10.1016/j.jastp.2009.12.012

Xiao, F. L., Zhou, Q. H., Su, Z. P., He, Z. G., Yang, C., Liu, S., He, Y. H., and Gao, Z. L. (2016). Explaining occurrences of auroral kilometric radiation in Van Allen radiation belts. *Geophys. Res. Lett.*, *43*(23), 11971–11978. https://doi.org/10.1002/2016GL071728

Xiao, F. L., Tang, J. W., Zhang, S., Zhou, Q. H., Liu, S., He, Y. H., Yang, Q. W., Kasahara, Y., Miyoshi, Y., ... Nakamura, S. (2022). Asymmetric distributions of auroral kilometric radiation in Earth's northern and southern hemispheres observed by the arase satellite. *Geophys. Res. Lett.*, *49*(13), e2022GL099571. https://doi.org/10.1029/2022GL099571

Yang, C., Wang, Z. Q., Xiao, F. L., He, Z. G., Xie, Y. Q., Zhang, S., He, Y. H., Liu, S., and Zhou, Q. H. (2022). Correlated observations linking loss of energetic protons to EMIC waves. *Sci. China Technol. Sci.*, *65*(1), 131–138. https://doi.org/10.1007/s11431-021-1882-x

Yang, Q. W., Yang, C., He, Y. H., Liu, S., Zhou, Q. H., and Xiao, F. L. (2016). Magnetospheric chorus wave instability induced by relativistic Kappa-type distributions. *Sci. China Technol. Sci.*, *59*(11), 1739–1745. https://doi.org/10.1007/s11431-016-0161-2

Zarka, P. (1998). Auroral radio emissions at the outer planets: Observations and theories. *J. Geophys. Res. : Planets*, *103*(E9), 20159–20194. https://doi.org/10.1029/98je01323

Zhang, S., Shang, X. J., He, Y. H., Liu, S., and Xiao, F. L. (2020). Dominant roles of high harmonics on interactions between AKR and radiation belt relativistic electrons. *Geophys. Res. Lett.*, *47*(16), e2020GL088421. https://doi.org/10.1029/2020GL088421

Zhang, S., Liu, S., Li, W. T., He, Y. H., Yang, Q. W., Xiao, F. L., Kumamoto, A., Miyoshi, Y., Nakamura, Y., ... Shinohara, I. (2021). A concise empirical formula for the field-aligned distribution of Auroral Kilometeric Radiation based on Arase satellite and Van Allen Probes. *Geophys. Res. Lett.*, *48*(8), e2021GL092805. https://doi.org/10.1029/2021GL092805

Zhang, S., Yin, Q. P., Yang, H. M., Xiao, F. L., Zhou, Q. H., Yang, Q. W., Tang, J. W., Deng, Z. K., Kasahara, Y., ... Hori, T. (2024). Direct observation of L-X mode of auroral kilometric radiation in the lower latitude magnetosphere by the arase satellite. *Geophys. Res. Lett.*, *51*(5), e2023GL105694. https://doi.org/10.1029/2023GL105694

Zhao, Y. W., Xiang, Z., Gu, X. D., Ni, B. B., Ma, X., Lou, Y. Q., Jiao, L. H., Zhou, R. X., Guo, D. Y., ... Dong, J. (2022). Simultaneous occurrence of four magnetospheric wave modes and the resultant combined scattering effect on radiation belt electrons. *Earth Planet. Phys.*, *6*(6), 563–575. https://doi.org/10.26464/epp2022050